Computer Graphics International 2011

Robust image-based 3D Modeling of Root Architecture

Luis D. Lopez · Deepak Shantharaj · Lu Liu · Harsh Bais · Jingyi Yu

Abstract Root system architecture (RSA) plays an important role in plant development and survival. The ability to accurately model and quantify properties of root architecture is fundamental for sustainability studies, crop improvement, and studies of plant-microbal interactions. Existing methods to model RSA either require a dense set of images or rely on 3D scanning methods for dense reconstruction. In this paper, we present an image-based technique for recovering complex 3D root geometry from a sparse set of viewpoints. Our solution incorporates 2D/3D root system topology as shape prior into the geometric reconstruction process. For every input view, we apply image matting for segmenting the root from the background. We then recover a $2D$ skeleton graph of the root from its matte image and find its corresponding 2D topology tree from the skeleton graph. Next, we present an iterative algorithm for computing the $3D$ topology tree that is most consistent with the set of $2D$ topology trees. Finally, we apply volumetric reconstruction for recovering the complete $3D$ root model from its 3D topology tree. We demonstrate our framework on roots of rice *(Oryza sativa)* and brachypodium *(B. distachyon)* and our experiments show that our method is robust and accurate.

Keywords Model Acquisition · Root Architecture · Three Dimensional Graphics · Image-based Modeling

L. D. Lopez
University of Delaware
E-mail: ldlopez@udel.edu

D. Shantharaj
University of Delaware
E-mail: deepaks@udel.edu

L. Liu
Washington University in St. Louis
E-mail: ll10@cse.wustl.edu

H. Bais
University of Delaware
E-mail: bais@dbi.udel.edu

J. Yu
University of Delaware
E-mail: jingyiyu@udel.edu

1 Introduction

Root system architecture (RSA) plays an important role in plant development and survival. Accurately recovering 3D root system architecture (RSA), however, is a challenging task and has received increasing attention from many research areas in recent years. Roots are difficult to model due to their highly complex branching structures and heterogenesis across species. Successful solutions for 3D root modeling have numerous applications in computer graphics/vision and plant science. For example, $3D$ root models can help plant scientists to identify and quantify plant growth dynamics and the effect of environmental factors in the development of plants. Recovering topological structures can also reveal new botanical information that leads to a more accurate simulation of the root system. Realistic $3D$ root models can also be used for physical-based simulation for scientific study, computer animations, and movie special effects.

In computer graphics, several approaches have been developed for producing realistic-looking root models, e.g., by using rule-based systems [8], fractals [24], physical simulations [14], or botanical rules [19]. Additional stochastic processes can model unpredictable changes in root growth [19]. Although these methods can generate naturally-looking roots, the synthesized root geometry can differ from the real one.

In computer vision, a few methods have been proposed for capturing 3D models of real roots. Most pre-

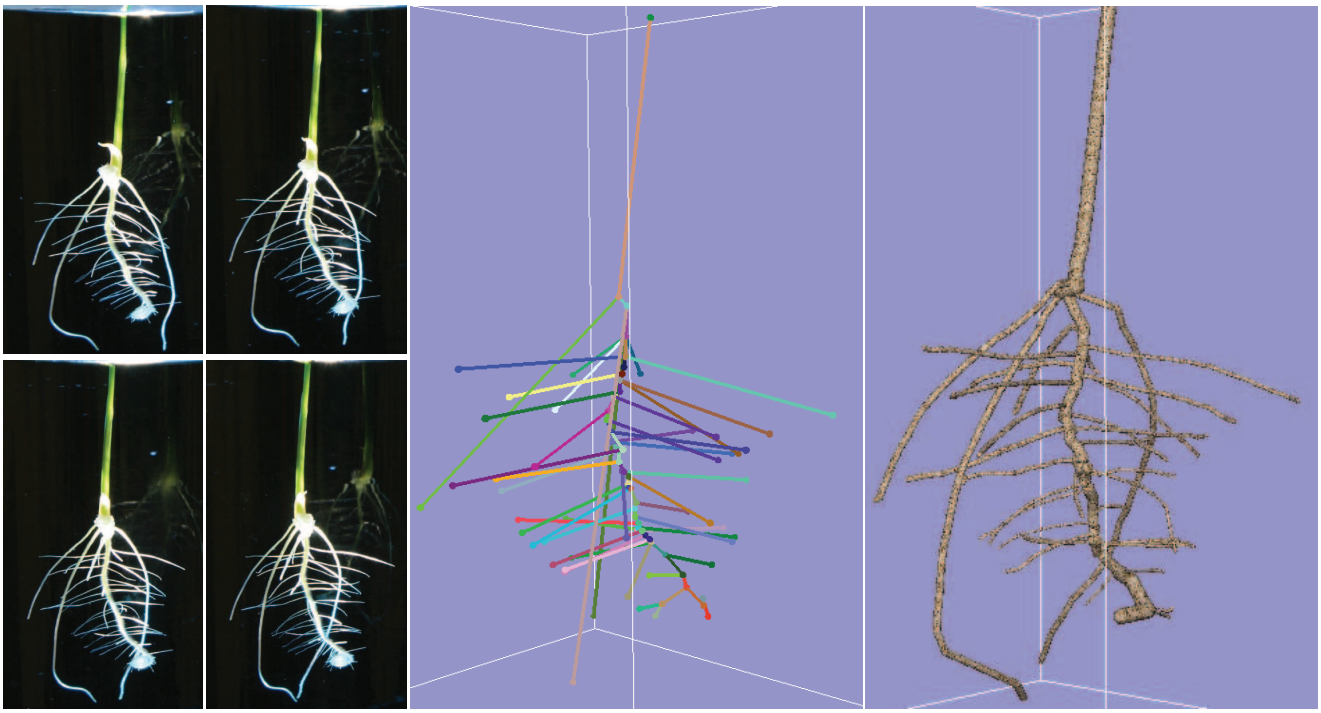

Fig. 1 Recovering a Root Architecture Model Using Our Approach. Left: four sample input images; middle: our recovered 3D Topology tree; right: our reconstructed 3D model.

vious work relies on computerized tomography (CT) technologies such as magnetic resonance imaging (MRI) [23], X-ray [20,4], or ground penetrating radar (GPR) [16] to obtain range data of the roots. These methods are able to observe the root in soil but require ad-hoc filtering techniques and additional processes to reconstruct the $3D$ model [28,34]. Further, they can be limited by cost, image resolution, and container size.

In this paper, we present an image-based technique for recovering complex 3D root geometry from a sparse set of viewpoints. Figure 2 illustrates our processing pipeline. We first construct an acquisition system for automatically capturing the images of the roots. We then select a small set of images for for reconstructing the $3D$ model. By using only a small number of input images, we minimize both user effects for root segmentation and computational cost for geometric processing. For every input view, we apply image matting for segmenting the root from the background. We then recover a $2D$ skeleton graph of the root from its matte image and find its corresponding 2D topology tree from the skeleton graph. Next, we present an iterative algorithm for computing the $3D$ topology tree that is most consistent with the set of $2D$ topology trees. Finally, we apply volumetric reconstruction for recovering the complete $3D$ root model from its 3D topology tree. We demonstrate our framework on roots of rice *(Oryza sativa)* and brachypodium *(B. distachyon)* and our experiments show that our method is robust and accurate.

2 Related Work

Most existing root modeling tools can be classified into two categories: synthesis methods and reconstruction methods.

Synthesis Methods: Approaches in this category focus on synthesizing the root geometry. Leitner et al. [7] generate the RSA using a small set of grammar-like generative rules called L-system. These rules are associated with dynamic parameters. By changing these parameters over time they synthesize different roots from the same initial parameters. Every set of rules constructs a specific type of root, and cannot be applied to new roots. De Willigen et al. [32] derived an analytical solution to model root growing as a two-dimensional diffusion process. They use different ratios of their diffusion coefficients to obtain roots with different shape and distribution patterns. Their volumetric results, however, do not reveal the actual geometric structures of real roots. Pages et al. [19] synthesized the RSA using a set of translations combined with morphogenetic rules. Realistic-looking roots are achieved by adding stochastic processes that model the unpredictable characteristics of the trajectories, branching factors, and size. It is important to note that all these approaches focus

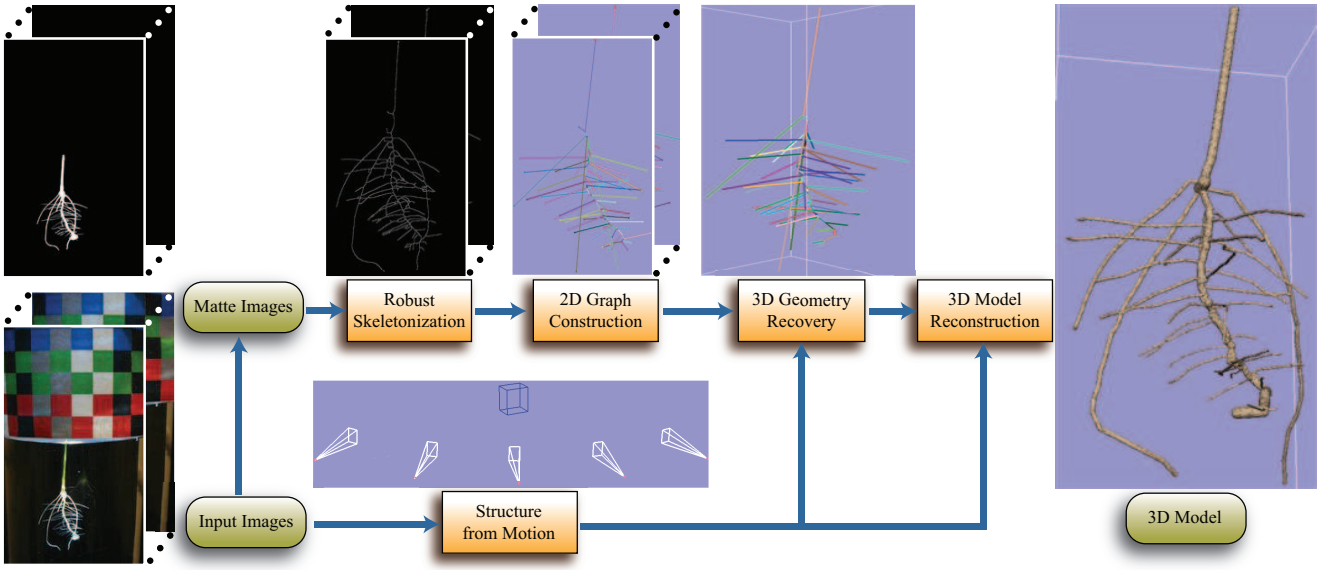

Fig. 2 Overview of Our Image-based Root Modeling System.

on visualization. Usually they assume an homogeneous distribution of the roots in the volume, and the synthesized tree geometry may differ greatly from the real one.

Reconstruction Methods: In contrast, reconstruction methods attempt to recover root geometry from actual roots. Gregory et al. [4] use a X-ray to acquire range data of roots rotating in a turntable. After filtering the density values to remove overlapping between the root, soil and container, they are able to recover an accurate volumetric model of the roots. MacFall et al. [23] capture $3D$ images using magnetic resonance imaging. Their approach reconstructs low resolution models. Similarly, Wielopolski et al. [16] use a ground penetrating radar to recover a volumetric model of large roots. Although computerized tomography technology can overcome the constraint imposed by opaque medium soil, these expensive devices have a limited resolution and require high imaging time, which makes it less suitable for large-scale application.Instead of computerized tomography, several approaches performed quantitative analysis of root architecture in $2D$ planes. For example, Liao et al [12] use a paper pouch system combined with image processing to analyze variation in root architecture on common beans. Devienne et al. [3] study the growth dynamic using a transparent wall technique to observe roots of Arabidopsis while they are growing in soil. Iyer-Pascuzzi et al. [22] use a turntable to capture a large number of images from fixed angles to perform a detailed measurement of several properties (e.g. root number, length, volume) of roots growing in a gel system. The main disadvantage of this method is that, it is not able to recover the $3D$ model. Lopez et al. [15] show that it is possible to recover real, instead of realistic-looking, $3D$ geometry of tree-like structures from a sparse set of images by using the skeleton trees as shape priors. We adopt a similar approach for finding the optimal $3D$ skeleton of the root that is most coherent with the $2D$ skeletons. We therefore briefly reiterate the main steps. The major difference is that their approach reconstructs the main trunks but is unable to recover tree geometry with fine details, whereas our solution can reconstruct micro-structures, such as root hairs that are important for characterizing their growth. Therefore, our method is more suitable to perform quantitative description and analysis on $3D$ root architecture from the recovered models. In line with our method Zhu et al. [29] reconstruct a visual hull from a large number of images surrounding the root. Their method is able to recover accurate volumetric models. The main disadvantages of their technique, however, are that by computing the $3D$ skeleton directly from the volume, they cannot guarantee connectivity and their method is susceptible to errors during segmentation and calibration. Similar to us Tian et al. [28] use a simple cylindrical representation derived from a volume space to model the root branches. Their method reconstructs realistic-looking roots. However, they only can recover vertical branches. In contrast by using a local volume space we are able to recover $3D$ root branches despite their orientation.

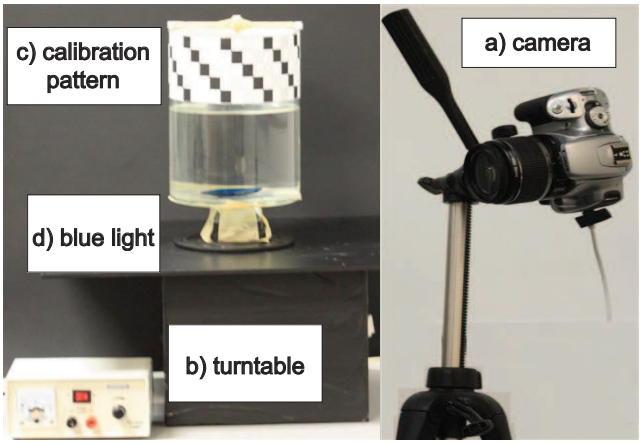

Fig. 3 Acquisition System.

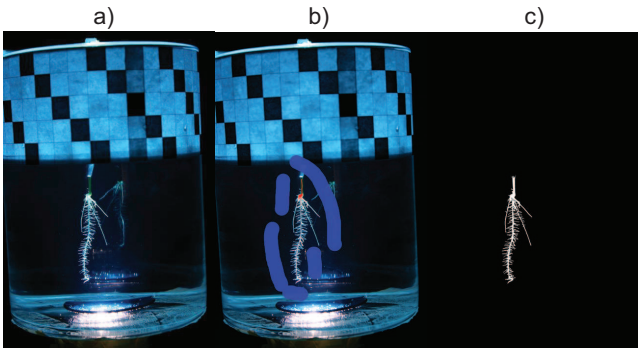

Fig. 4 Matte estimation using [31] algorithm (A) Input Image; (B) User Input Strokes; (C) Estimated Alpha Matte.

3 Preliminary Processing

3.1 Plant Growth

In this paper, we use rice *(Oryza sativa)* and brachypodium *(B. distachyon)* for reconstructing root system architecture. We follow standard procedures to grow the seeds in gel system. Specifically, we dehusk the seeds to remove surface borne pathogens, sterilize them with 50% sodium hypochlorite for 5 mins, and then rinse them three times with sterile water. Sterilized seeds grow in a vented tissue culture flask $75cm^2$ filled with growth medium consisting full strength MS and 0.15% phytagel (pH-5.8). Plants grow at room temperature with a photoperiod of $12 - hr$ day/night. Finally we separate the rice from the gel after 15 days and the Brachypodium after 30 days.

3.2 Image Acquisition and Camera Pose Recovery

We developed an acquisition system (figure 3) that consists of the following devices:

- a single CCD-camera (figure 3a), Canon EOS Digital Rebel Xti SLR camera with 55 mm focal length and a resolution of 2592x3888 pixels.
- a turntable (figure 3b) used to obtain multiple views of the roots, with $20cm$ of diameter, its position can be specified with an accuracy of 1.0^o.
- a calibration pattern (figure 3c) used to extract point correspondence and run structure-from-motion on them to recover camera parameters.
- a blue-light lamp (figure 3d) used to illuminate the root during acquisition.

We capture a dense set of viewpoints with 90^o coverage around the root. We then obtain the camera calibration matrix for each view, using the approach described in [17]. One of the main problems during calibration is that branches of roots have very similar colors and textures, and appearance can vary significantly across views due to changes in occlusion patterns. To resolve this problem, we only extract point correspondences from the calibration pattern in the acquisition system. We then select a sparse set of images from the dense set of viewpoints to use in the following processes. We do that because even with advanced segmentation [21,5] and matting tools [31,11], segmenting a large number of images is time consuming and tedious. Therefore, we pursue a solution that uses much fewer images.

Similar to the image-based method for the automatic phenotyping of root systems [22], we start with segmenting the foreground root from the background region. However, we choose to find a smooth alpha matte of the root while [22] uses an adaptive thresholding technique for segmentation. This is because roots contain thin secondary branches with intricate boundaries that blend into the background and are difficult to segment using standard thresholding techniques. The alpha matte, instead, can capture these small details and is consistent with our approach for finding the root topology (Section 4). Several techniques have been developed to estimate the alpha matte of an image [21,26, 9,10,30]. In our experiments we use the Robust Matting technique proposed by Wang et al. [31]. This method allows the user to draw foreground and background strokes and progressively refine the alpha matte. Figure 4 shows the recovered alpha matte of a sample input image.

4 Recovering 2D Root Topology

4.1 Robust 2D Skeleton Graph

Similar to the image-based approach by Zhu et al. [29], we use the skeleton to describe the shape and topology of the roots. Their method computes coarse skeletons

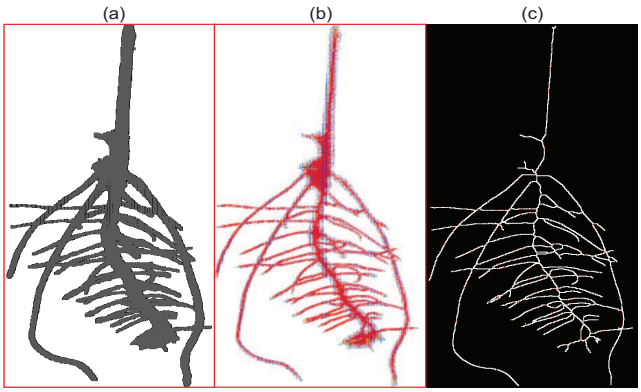

Fig. 5 Robust Skeletonization using [13] algorithm (A) Input Cell Complex; (B) Medial Persistence MP from (A); (C)Skeleton Graph computed by simple, iterative cell removal

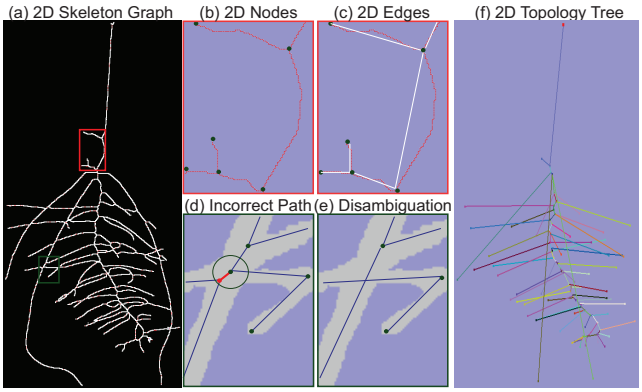

Fig. 6 Reconstruction of 2D Skeleton Trees from 2D Graphs (A) An Input 2D Skeleton Graph; (B) to (D): We identify the nodes of the Skeleton Tree and their connectivity; (E) We fix the incorrect paths;(F) Our final recovered 2D Skeleton Tree

from the volumetric model. Unlike [29] we compute fine skeleton graphs by using high resolution images. Our solution is robust to noisy boundaries, and we can guarantee the connectivity in our reconstructed model.

In our solution the matte image is converted to a cell complex [33]. For every pixel in the foreground region, we create a $3D$ cube by mapping its image position to a normalized device coordinate (NDC) system in two parallel planes. Neighboring pixels share points used to create the edges that define one of their six faces.

To extract the skeleton graph from the cell complex, we directly use the robust thinning algorithm developed by Liu et al. [13]. The thinning algorithm formulated a skeleton significance measure, called *medial persistence*. Guided by this measure, the previous algorithm produces a family of topology and shape preserving skeletons whose shapes and composition can be flexibly controlled by the desired level of medial persistence. Figure 5 shows the skeleton graph (Fig. 5c) extracted from a sample input image (Fig. 5a).

4.2 Construction $2D$ Topology Tree from Graph

The previous section described how the skeleton graph is extracted from the matte image. Given the skeleton graph, we construct its corresponding $2D$ topology tree. To do so, we first convert the skeleton graph into an undirected graph where the nodes are defined by leaves and junctions in the skeleton graph (Fig. 6b). We use the connectivity of the points in the skeleton to identify the leaf and junction nodes. Leaf nodes are detected by finding the endpoints, while the junction nodes correspond to the 3-connected and 4-connected points in the skeleton. We then find the edges that connect the nodes in the undirected graph by removing the interior points in the path between every pair of connected nodes (Fig. 6c).

Finally, we identify and discard the multi-furcation points that are caused by occlusions between the branches (Fig. 6d). To do so, from the matte image, we compute a distance field [1]. For each pixel p, we compute its shortest distance to the boundary (i.e., pixels whose alpha value is zero) and map the corresponding distance to the nodes in the undirected graph. We then check for every pair of connected nodes with the same degree and an Euclidean distance smaller than their distance field value. If this is the case, those nodes correspond to a branch intersection, and we need to remove the nodes and fix the connectivity. We do that, by first removing the edge that connects them, then checking the angle between the remaining edges, and finally applying a Greedy algorithm to find the optimal connectivity that yields the highest angle consistency. In the rare case when multiple branches occlude each other at the same point, it is highly challenging to automatically correct the connectivity between the nodes. Therefore, our framework allows users to manually fix the connectivity in such cases.

5 $3D$ Root Topology Recovery

We next proceed to compute the $3D$ topology tree that is most consistent with the set of $2D$ topology trees. The core of our approach is to match a pair of trees. We developed an iterative tree matching technique inspired by the recent approach proposed by Charnoz et al. [2] that estimates the optimum match between two skeleton trees, computed from CT-scan images, using geometric and topological cues. The major difference between the two approaches is that, rather than discarding solutions based on their cost, we use a simple but efficient dynamic pruning technique that only discards unfeasible solutions. As shown in the results sec-

tion our approach is able to find the global solution while controlling the growth of the search space.

Pairwise Tree Matching Given two $2D$ topology trees t^{left} and t^{right} we first compute the matching cost between all pairs of nodes across the trees. For simplicity, we use l_i to denote the $i-th$ node in t^{left}, and r_j to represent the $j-th$ node in t^{right}. our goal is to use geometric and topological attributes to compute the optimum match between their respective nodes.

Our approach to compute the matching cost is based on the observation that a pair of $2D$ trees correspond to the same $3D$ tree observed from different viewpoints. Therefore, if a pair of nodes match, they should correspond to the same $3D$ point. Thus, For a given pair of nodes l_i and r_j we compute their matching cost as the minimum distance between their corresponding rays in $3D$ space $C(i,j) = d_{i,j}$, where the rays are computed from the recovered camera parameters (figure 7a). If this cost is too large, then it indicates that the two rays do not intersect, and we simply mark the cost as infinity $C(i,j) = \infty$. If the midpoint of the minimal distance segment $Q_{i,j}$ lies out of a pre-defined bounding frustum, we also mark the cost as infinity as it indicates an incorrect correspondence. We also discard correspondences by considering a local window. If the $2D$ Euclidean distance between the pair of nodes is too large, we mark the cost as infinity.

Once we finish building the cost matrix we start matching the nodes by constructing a hypothesis tree using a breadth-first search approach. Every node in the hypothesis tree consists of a likely solution of the matching problem. We initialize our algorithm by assuming that the root nodes l_0 and r_0 always match and make their match as the root of the hypothesis tree. Starting at the root node, for each matching pair (l_i, r_j) we enumerate all combinations of possible matches between their child nodes $(CH(l_i), CH(r_j))$ as hypothesis nodes(figure 7b). Since partial occlusion or other geometric artifacts can change the connectivity between the topology trees in some intermediate nodes, we need to consider potential matches in subtrees and not only in child nodes. To resolve this issue we also consider the hypothesis of matching grandchild nodes $GCH(l_i)$ and $GCH(r_j)$ against the child nodes $CH(l_i)$ and $CH(r_j)$ respectively. If a specific hypothesis node contains a matching pair with ∞ matching cost, we simply discard that node. In some cases, the number of the children nodes in the two trees is not equal. For example one has three children nodes, the other has two. In these cases, we insert special empty nodes to match the number of children. This usually happened when a branch appears in one view but its occluded in the other. Finally the optimal matching combination corresponds to

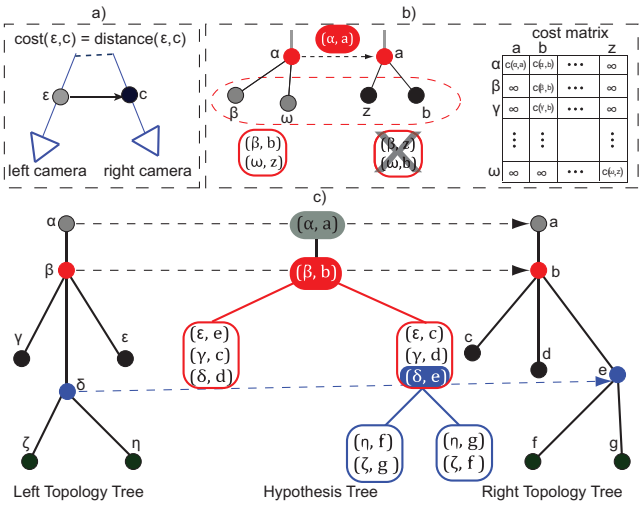

Fig. 7 Pairwise Topology Tree Matching; (A)Computing matching cost (B)Pruning Hypothesis Tree using the Cost Matrix; (C) Growing the Hypothesis Tree

the leave node in the hypothesis tree with the minimum overall accumulated cost.

3D Tree Construction To reconstruct the $3D$ topology tree we first pick the $2D$ tree that captures most visible branches as reference and apply our pairwise matching algorithm between this reference tree and the rest of the input $2D$ topology trees. This significantly reduces the computational cost. Then, for every node in the reference tree, we find its corresponding node in the rest of the skeleton trees and apply triangulation. We then create a $3D$ node by computing the centroid of the set of $3D$ points from triangulations. Finally, we construct the $3D$ Tree by connecting the recovered 3D nodes using the topology of the reference tree. Fig 9 shows several $3D$ skeleton trees recovered by our method.

6 Model Recovery

Once we recover the optimum $3D$ topology tree, we apply a revised volumetric reconstruction approach to recover the complete model of the root. For each edge in the $3D$ topology tree, our approach applies a space carving method on a local volume to estimate the branch geometry (e.g., shape and size). Our solution is based on the observation that topology tree casts important geometry constraints. Therefore, by actively integrating the recovered $3D$ topology tree as shape priors we effectively reduce the initial volume size. Furthermore we show that unlike the classical visual hull approach, our technique is still able to faithfully and robustly recover high quality root geometry even employing few input viewpoints.

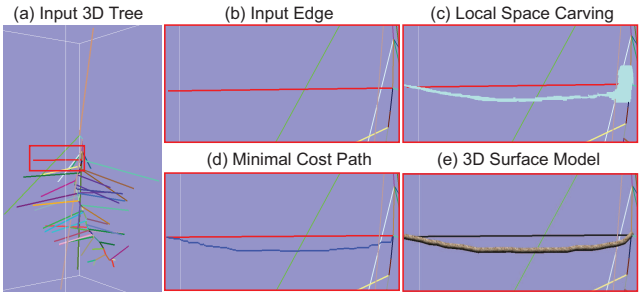

Fig. 8 Topology-driven Model Reconstruction

6.1 Per-Branch Cylindrical Modeling

Classical volumetric approaches [18,6] reconstruct the shape of complex objects by first covering the scene with a $3D$ space by intersecting the view frustums of all cameras. This space is then discretized into voxels. The sampling resolution of the discrete $3D$ space is limited by the input image size. Notice that in order to recover fine details from the input images, large image resolution needs to be used for discretization (e.g., 3Kx4K in our case). and the resulting volume size would be too large to process or store. To fix these problems, existing volumetric-based modeling methods trade off volume resolution for processing speed, and they are only able to recover coarse geometry [25].

Our technique, instead, resolves the resolution issue by directly using the recovered $3D$ topology tree to guide a local volume discretization. Specifically, we use a $3D$ cylinder to bind each branch. The radius of the cylinder is chosen to be large enough to cover all pixels of the branch when back-projected onto the views. We then discretize each cylinder into voxels at a resolution of twice the image resolution to avoid undersampling. Since each branch only covers a small amount of pixels, our method significantly reduces the initial volume size. In our experiments, the size of our cylinder volume representation is usually only 5 percent or less of the standard view frustum discretization.

Next, we directly apply space carving on each discrete cylindrical volume (Fig. 8c). For each voxel inside the cylinder, we project it back to all input images. To further reduce the computational overhead, we simply carve out the voxel if its corresponding pixel lies in the background of the matte image in any views.

To recover the actual branch geometry, classical volumetric reconstruction [6] could be applied to refine the volume. However, since we only use very few views, the volumetric results are usually very noisy. Therefore, we use a piece-wise cylindrical model to represent the actual $3D$ root geometry. This representation seems to be a more natural fit to branches, requires less memory, and allows the visualization of the model without any special hardware. Specifically, we first locate two voxels that correspond to the endpoints of the branch edge in the $3D$ topology tree. We then use Fast March algorithm [27] to compute the optimal path between the two nodes. Finally, we approximate the branch geometry by concatenating cylinders along the pass. To estimate the cylinder radius, at every voxel V on the optimal path, we first estimate a local cut plane and find all uncarved voxels lying on the plane. We further find the minimum distance from V to the edge and use it as the radius of the curved cylinder to approximate the $3D$ branch. Since we use the minimum distance to the peripheral voxels, our estimated radius tends to be smaller than its actual value. Figure (8e) shows our reconstruction result of a sample branch on a rice's root. We refer the readers to the supplementary video to view the complete model.

7 Results

We demonstrate our framework on recovering $3D$ root architecture models for a variety of roots with different shape and density of branches. In all our experiments, we only use four images covering 90^0 around the root. The images were captured using the acquisition device as discussed in Section 3.2. Root imaging took about 5 minutes for each root.

We conduct our reconstruction algorithms on a DELL PC with Intel Core i7 2.8Ghz CPU and 8GB of RAM. Computational time for reconstruction depends on the complexity of the root. The resolution of the input images is 2592×3888. We use full image resolution in all the processes. For camera calibration, our structure from motion algorithm takes approximately 1 minute on average for each input sequence. Segmenting the image using Robust Matting algorithm [31] takes about 2 minutes per image for the user to specify the strokes and obtain the mattes. Recovering the $2D$ topology tree takes about 10 seconds for each input image. On average our algorithm to reconstruct the $3D$ topology tree described in Section 5 takes less than 2 seconds for each tree. Generating the cylindrical model takes about 20 to 40 seconds depending on the number of branches in the root. Table 1 summarizes the image resolution (after cropping) and the number of branches recovered from the input images.

Rice. The first row of Figure 9 shows a rice root reconstructed by our algorithm. This root has four large broad primary branches. One of these primary branches has a curved cap holding several large and thin lateral roots with complex occlusion patterns. These properties make it challenging for segmentation and topology recovery processes. In this experiment an user needs to

Table 1 Root information in our experiments

Sequence	Resolution	Num branches	Recovered
Rice	668×1180	46	39
Brachypodium	700×800	10	10
Rice EA-104	800×950	57	46

manually remove the leaf-like surface (Scutellum) that covers the seed, and we can automatically recover the $2D$ topology trees without user intervention. Column (a) shows the view that we pick for $3D$ reconstruction. Column (b) shows the reconstructed $3D$ topology tree. Columns (c) and (d) show the geometry of our recovered model. Our method accurately recovers all the primary branches and about 80% of the secondary branches. Most of the missed branches occur when thin roots are clusterized in small zones. When several branches are close to each other, it is not easy to determine their correspondence in the other views; therefore, our algorithm can incorrectly associate a node in the reference view with the children or grandchildren node of the correct match, creating fake gaps. We refer the reviewers to the supplementary video for the complete $3D$ model recovered by our algorithm.

Brachypodium. The second row of Figure 9 shows our reconstruction results on a Brachypodium root. This root has only two large broad primary branches and few secondary branches. All the branches contain thousands of hairs that merge with the background. These features make the modeling process easy and the segmentation process very challenging. We minimize the effect of root hairs by setting a high threshold to binarize the matte images. Topology extraction and $3D$ modeling are straightforward. Notice that although several branches are strongly curved, our method is able to accurately recover the $3D$ geometry of all the branches.

Rice EA-104. In the bottom row of Figure 9, we apply our reconstruction method on a rice treated with a bacteria (EA-104) that inhibits the growing of their branches. Similar to the regular rice, it has few large primary branches, and one primary branch with a curved cap holding several short and thin lateral branches. The segmentation was fully automatic, but we require more user interaction in the $2D$ topology recovery process to fix the connectivity in several branches due to complex occlusion. Our technique recovered very accurate geometry of all the primary branches and most of the lateral roots. In all three examples, our approach is able to reconstruct accurate models that comprise the root topology and with a geometry consistent with the input images.

8 Conclusions and Discussions

We have presented an image-based solution for reconstructing $3D$ root models from images. Our method is able to recover accurate $3D$ geometry using a sparse set of images. The core of our approach is to guide the modeling process imposing $2D$ and $3D$ root topology information as shape priors. Specifically, we have developed an iterative matching algorithm to combine $2D$ topology trees from different views and recover the most consistent $3D$ root topology. We have then used the reconstructed $3D$ topology tree to guide per-branching cylindrical modeling for recovering the complete geometry of the roots. We have demonstrated our framework on a variety of plants. Our results have shown that our method is robust, accurate and reliable.

There are several future directions for improving our current implementation. For instance, one limitation of our approach is that we pick the image that contains most visible branches as the reference view for recovering the $3D$ topology tree, and if a branch is missing in the reference view, we will not be able to recover it. In the future we plan to study more complex $2D$ topology tree matching algorithm that can recover the branches observed from any view.

Another promising direction of future research is incorporate traditional segmentation techniques in the matting algorithm to automatically segment the roots from the background. In particular, we plan to use intensity information to automatically generate the trimap image for the image matting algorithm and use an iterative approach to refine the segmentation results.

An apparent limitation of our technique is that it cannot handle clusters of branches. In our framework, a pure geometric approach to construct the optimum $3D$ topology tree can generate fake gaps in the reconstructed model. One possible solution is to explore other heuristics to rank the nodes in the hypothesis tree. Our algorithm is purely image-based and does not use botanical information. In the future, we also plan to integrate botanical information to increase the performance in the $3D$ topology reconstruction. For example, we can conduct a template matching to find similar parametric models and use this information to improve the reconstructed topology.

Acknowledgements We would like to thank the CGI anonymous reviewers for their comments and suggestions. This work is partially supported by the NSF under grants IIS-CAREER-0845268 and IIS-RI-1016395, and Conacyt under grand 171570.

References

1. Borgefors, G.: Distance transformations in digital images. Comput. Vision Graph. Image Process. **34**(3), 344–371 (1986)
2. Charnoz, A., Agnus, V., Malandain, G., Nicolau, S., Tajine, M., Soler, L.: Design of robust vascular tree matching: Validation on liver. In: G. Christensen, M. Sonka (eds.) Information Processing in Medical Imaging, *Lecture Notes in Computer Science*, vol. 3565, pp. 443–455. Springer Berlin Heidelberg (2005)
3. Devienne-Barret, F., Richard-Molard, C., Chelle, M., Maury, O., Ney, B.: Ara-rhizotron: An effective culture system to study simultaneously root and shoot development of arabidopsis. Plant and Soil **280**, 253–266 (2006)
4. Gregory, P., Hutchison, D.J., Read, D.B., Jenneson, P.M., Gilboy, W.B., Morton, E.J.: Non-invasive imaging of roots with high resolution x-ray micro-tomography. Plant and Soil **255**, 351–359 (2003)
5. Kolmogorov, V., Zabih, R.: What energy functions can be minimized via graph cuts? In: ECCV '02: Proceedings of the 7th European Conference on Computer Vision-Part III, pp. 65–81. London, UK (2002)
6. Kutulakos, K., Seitz, S.: A theory of shape by space carving. IJCV **38**(3), 199–218 (2000)
7. Leitner, D., Klepsch, S., Bodner, G., Schnepf, A.: A dynamic root system growth model based on l-systems. Plant Soil **332**, 177–192 (2010)
8. Leitner, D., Schnepf, A.: Root growth simulation using l-systems. pp. 313–320 (2009)
9. Levin, A., Lischinski, D., Weiss, Y.: A closed-form solution to natural image matting. IEEE Trans. Pattern Anal. Mach. Intell. **30**, 228–242 (2008)
10. Levin, A., Rav-acha, A., Lischinski, D.: Spectral matting. In: In CVPR (2007)
11. Li, Y., Sun, J., Tang, C.K., Shum, H.Y.: Lazy snapping. In: SIGGRAPH '04: ACM SIGGRAPH 2004 Papers, pp. 303–308. ACM, New York, NY, USA (2004)
12. LIAO Hong, Y.X.L.: Adaptive changes and genotypic variation for root architecture of common bean in response to phosphorus deficiency. pp. 158–163 (2000)
13. Liu, L., Chambers, E., David, L., Tao, J.: A simple and robust thinning algorithm on cell complexes. In: Proceedings of Pacific Graphics 2010, vol. 29, pp. 2253–2260 (2010)
14. Logvenkov, S.A.: Modeling plant root growth. Fluid Dynamics **28**, 69–75 (1993)
15. Lopez, L.D., Ding, Y., Yu, J.: Modeling complex unfoliaged trees from a sparse set of images. Computer Graphics Forum **29**, 2075–2082(8) (September 2010)
16. Lucian, W., George, H., Jeff, D., Michael, M.: Imaging tree root systems in situ. In: Proceedings of 9th International Conference on GPR, vol. 4758, pp. 58–62 (2002)
17. Luong, Q., Faugeras, O.: Self-calibration of a moving camera from point correspondences and fundamental matrices. IJCV **22**(3), 261–289 (1997)
18. Matusik, W., Buehler, C., Raskar, R., Gortler, S.J., McMillan, L.: Image-based visual hulls. In: Proceedings of the 27th annual conference on Computer graphics and interactive techniques, SIGGRAPH '00, pp. 369–374. ACM Press/Addison-Wesley Publishing Co., New York, NY, USA (2000)
19. Pagés, L.: Root system architecture: from its representation to the study of its elaboration. pp. 295–304 (1999)
20. Pierret, A., Kirby, M., Moran, C.: Simultaneous x-ray imaging of plant root growth and water uptake in thin-slab systems. Plant and Soil **255**, 361–373 (2003)
21. Rother, C., Kolmogorov, V., Blake, A.: "grabcut": interactive foreground extraction using iterated graph cuts. In: SIGGRAPH '04, pp. 309–314 (2004)
22. S., I.P.A., Olga, S., Yuriy, M., Yueling, H., Heather, B., John, H., S., W.J., N., B.P.: Imaging and analysis platform for automatic phenotyping and trait ranking of plant root systems. Plant Physiology (3), 152:1148–57 (2010)
23. S., M.J.: Visualization of root growth and development through magnetic resonance imaging. Radical Biology: Advances and Perspectives on the Function of Plant Roots (Flores H E, Lynch J P, Eissenstat D, eds) pp. 57–80 (1997)
24. Shibusawa, S.: Modelling the branching growth fractal pattern of the maize root system. Plant and Soil **165**, 339–347 (1994)
25. Slabaugh, G., Culbertson, B., Schafer, R., Malzbender, T.: A survey of methods for volumetric scene reconstruction from photographs pp. 81–100 (2001)
26. Sun, J., Jia, J., keung Tang, C., yeung Shum, H.: Poisson matting. ACM Transactions on Graphics **23**, 315–321 (2004)
27. Telea, A., van Wijk, J.J.: An augmented fast marching method for computing skeletons and centerlines. In: VISSYM '02: Proc. of the symposium on Data Visualisation, pp. 251–ff. Eurographics Association, Aire-la-Ville, Switzerland (2002)
28. Tian, X., Han, G., Chen, M., Situ, Z.: Skeleton-based surface reconstruction for visualizing plant roots. International Conference on Artificial Reality and Telexistence **0**, 328–332 (2006)
29. Tonglin, Z., Suqin, F., Zhiyuan, L., Yutao, L., Hong, L., Xiaolong, Y.: Quantitative analysis of 3-dimensional root architecture based on image reconstruction and its application to research on phosphorus uptake in soybean. pp. 2351–2361 (2006)
30. Wang, J., Agrawala, M., Cohen, M.F.: Soft scissors: an interactive tool for realtime high quality matting. In: ACM SIGGRAPH 2007 papers, SIGGRAPH '07. ACM, New York, NY, USA (2007)
31. Wang, J., Cohen, M.F.: Optimized color sampling for robust matting. In: Computer Vision and Pattern Recognition, 2007. CVPR '07. IEEE Conference on, pp. 1–8 (2007)
32. Willigen, P.D., Heinen, M., Mollier, A., Noordwijk, M.V.: Two-dimensional growth of a root system modelled as a diffusion process. i. analytical solutions. Plant and Soil **240**, 225–234 (2002)
33. yi Zhou, Q., Ju, T., min Hu, S.: Topology repair of solid models using skeletons. IEEE Transactions on Visualization and Computer Graphics pp. 675–685 (2007)
34. Zhou, X., Luo, X.: Advances in non-destructive measurement and 3d visualization methods for plant root based on machine vision. In: BMEI, pp. 1–5 (2009)

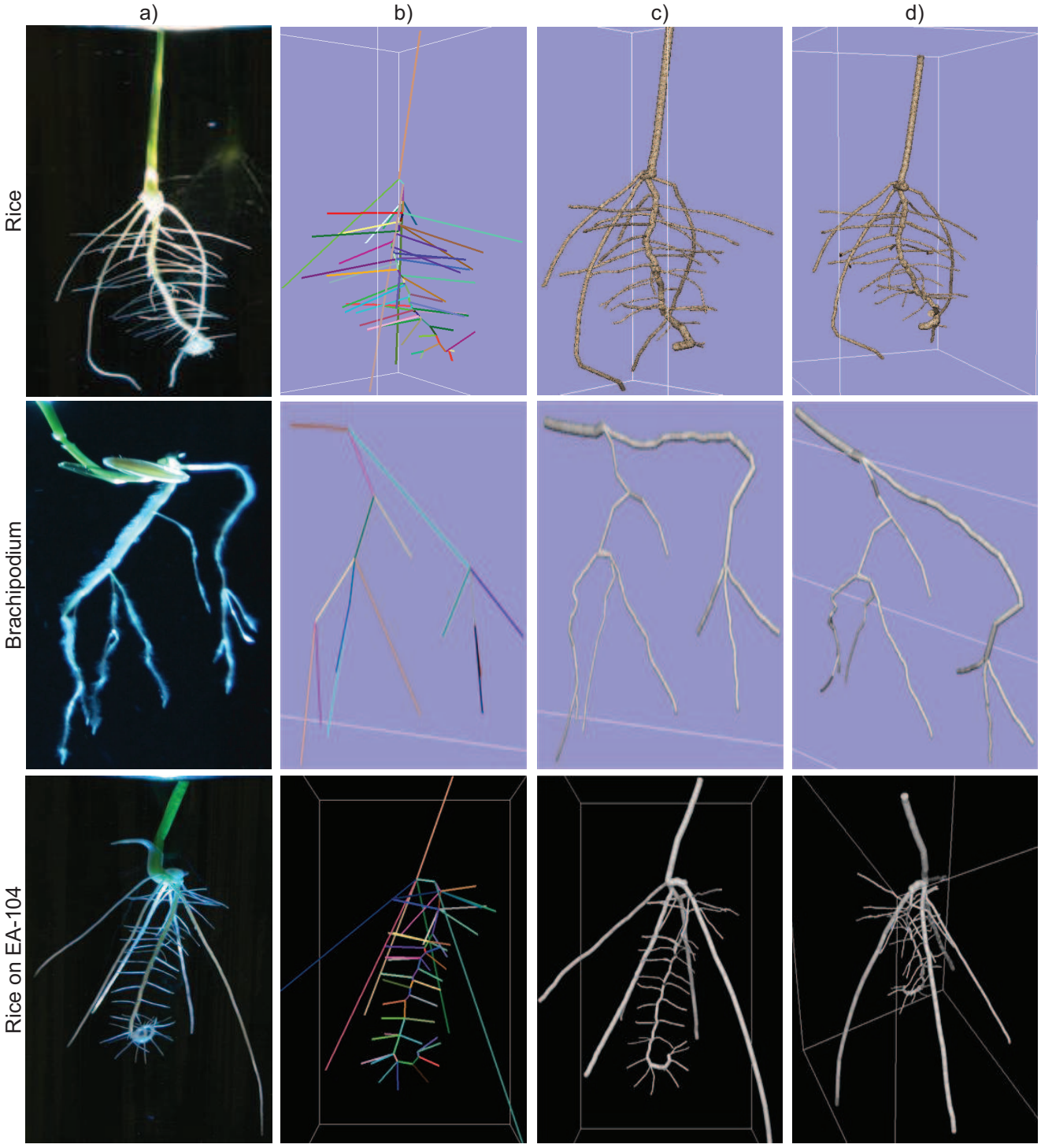

Fig. 9 3D Models Generated by Our Framework. (a): The reference view used for reconstruction. (b) The recovered topology tree. (c) and (d): Two views of our final reconstructed $3D$ root architecture model. Each model is reconstructed using only 4 input images.